**The EMBO Journal** Vol.17 No.8 pp.2378–2391, 1998

# Tertiary structure formation in the hairpin ribozyme monitored by fluorescence resonance energy transfer

**Nils G.Walter, Ken J.Hampel, Kirk M.Brown and John M.Burke[1]**

Markey Center for Molecular Genetics, Department of Microbiology and Molecular Genetics, The University of Vermont, Burlington, VT 05405, USA

[1]Corresponding author
e-mail: jburke@zoo.uvm.edu

**The complex formed by the hairpin ribozyme and its substrate consists of two independently folding domains which interact to form a catalytic structure. Fluorescence resonance energy transfer methods permit us to study reversible transitions of the complex between open and closed forms. Results indicate that docking of the domains is required for both the cleavage and ligation reactions. Docking is rate-limiting for ligation ($2\ min^{-1}$) but not for cleavage, where docking ($0.5\ min^{-1}$) precedes a rate-limiting conformational transition or slow-reaction chemistry. Strikingly, most modifications to the RNA (such as a $G_{+1}A$ mutation in the substrate) or reaction conditions (such as omission of divalent metal ion cofactors) which inhibit catalysis do so by preventing docking. This demonstrates directly that mutations and modifications which inhibit a step following substrate binding are not necessarily involved in catalysis. An improved kinetic description of the catalytic cycle is derived, including specific structural transitions.**

*Keywords*: catalytic RNA/domain docking/metal ions/reaction mechanism/RNA folding

## Introduction

The hairpin ribozyme is an endonucleolytic RNA motif 50 nucleotides in length that was first discovered in the negative strand of the tobacco ringspot virus satellite RNA (Buzayan *et al.*, 1986; Feldstein *et al.*, 1989). The naturally occurring *cis*-acting ribozyme can be truncated and converted to act *in trans* by deletion of sequences that are not required for substrate recognition and catalysis (Hampel and Tritz, 1989). *Trans*-acting hairpin ribozymes have been used by several groups to explore structure–function relationships (reviewed in Burke *et al.*, 1996; Earnshaw and Gait, 1997), and to investigate their use for selective inhibition of mammalian gene expression (reviewed in Welch *et al.*, 1996).

The secondary structure of the hairpin ribozyme has been established through the analysis of limited phylogenies derived from natural evolution (DeYoung *et al.*, 1995), more extensive phylogenies derived from *in vitro* selection (Berzal-Herranz *et al.*, 1993), and through mutational studies (Anderson *et al.*, 1994). The ribozyme–substrate complex is comprised of two independently folding domains termed A and B, each consisting of an internal loop flanked by two short helices. The substrate binds to domain A through helices 1 and 2, and becomes reversibly cleaved within internal loop A (Figure 1A). Notably, the identity of virtually all bases within the two internal loops is important for activity of the ribozyme. In contrast, the sequence of the four helices can vary widely, provided that Watson–Crick base-pairing is maintained.

Two lines of experimental evidence point to the importance of a specific interaction between the two domains. First, the introduction of variable-length linkers between the 5′ end of the substrate and the 3′ end of the ribozyme showed that constraining helices 2 and 3 to a coaxial stack eliminates catalytic activity (Feldstein and Bruening, 1993; Komatsu *et al.*, 1994). Kinetic and conformational analyses showed that the standard *trans*-ribozyme construct can adopt an analogous structure that represents a misfolded conformational isomer (Esteban *et al.*, 1997, 1998). Secondly, we have shown that catalytic activity can be reconstituted following separation of the two domains (Butcher *et al.*, 1995). At high RNA concentrations, cleavage activity approaches that of the unmodified ribozyme, suggesting that the interdomain tertiary interactions are specific, but relatively weak.

Exploration of the interactions between the two domains has begun only recently. A tertiary structure model of the hairpin ribozyme has been developed from published biochemical data and new cross-linking results (Earnshaw *et al.*, 1997). In this molecular model, interdomain contacts include specific contacts between the 2′ hydroxyl groups of essential ribose moieties within helix 2 of domain A, and partners in loop B.

The reactions catalyzed by the hairpin ribozyme are known to be stimulated by metal ions (Hampel and Tritz, 1989; Chowrira *et al.*, 1993a) as is the case for other small ribozymes that generate 2′,3′ cyclic phosphates, including the hammerhead, hepatitis delta and *Neurospora* VS ribozymes (Sigurdsson *et al.*, 1998). Magnesium ions are likely to be the most important metal ions that support catalysis in the biological environment. Although divalent metal ions have been thought to play an essential role in reaction chemistry, two recent results have brought this into question. First, cobalt (III) hexammine can fully support folding and catalysis by the hairpin ribozyme, despite the fact that its fully occupied and stably coordinated ligand shell precludes inner-sphere contacts between the metal ion and any component of the RNA (Hampel and Cowan, 1997; Nesbitt *et al.*, 1997; Young *et al.*, 1997). Secondly, we have found that high levels of catalytic activity can be obtained for the hairpin, hammerhead and VS ribozymes using monovalent salts in the presence of chelating agents (J.B.Murray, A.A.Seyhan, J.M.Burke and W.G.Scott, in preparation). The function of metal ions in

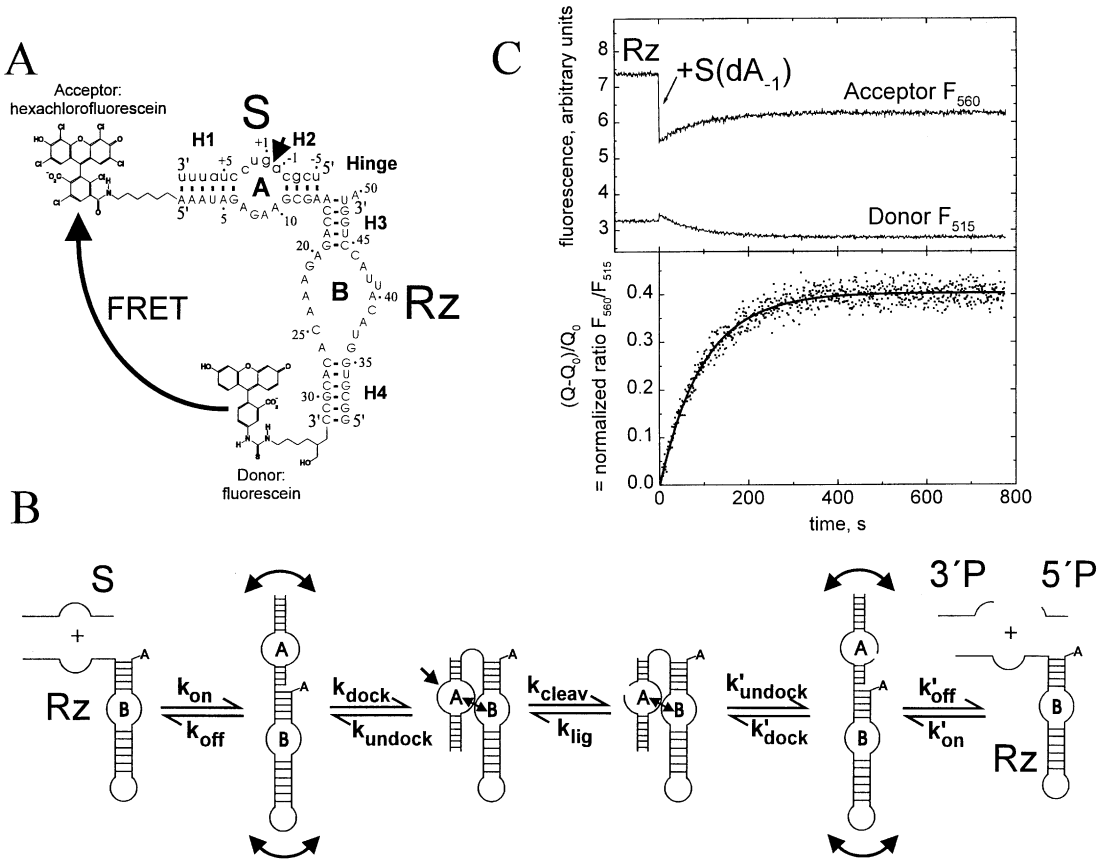


**Fig. 1.** Kinetics of tertiary structure formation in the hairpin ribozyme–substrate complex can be monitored by FRET. (**A**) The double-labeled ribozyme–substrate complex utilized for energy transfer measurements. The two-strand hairpin ribozyme (Rz, capital letters) binds the 14-nucleotide substrate (S, small letters) to form the A domain comprising helices 1 and 2, and the symmetric internal loop A. This part of the molecule is connected via a flexible 'hinge' to the B domain of the ribozyme containing helices 3 and 4, and an asymmetric internal loop B. Fluorescein and hexachlorofluorescein are coupled as donor–acceptor pair to the 3′- and 5′-ends of the 5′ half of the two-strand ribozyme to enable distance-sensitive FRET (curved arrow). The short arrow indicates the potential cleavage site. (**B**) Schematic representation of a minimal kinetic mechanism for hairpin ribozyme catalysis as revealed by the current study. Substrate *in trans* (S) is bound by the ribozyme (Rz) into an open, extended conformation. This structural conformer is flexible enough (curved arrows) to fold into a docked, bent structure, enabling loops A and B to interact. Subsequently, site-specific cleavage occurs (short arrow), the complex unfolds into an open complex and the 5′ and 3′ cleavage products (5′P and 3′P) dissociate. All steps are fully reversible and can be characterized by individual rate constants as indicated. It is notable that there might be additional steps involved in catalysis, such as other structural changes, to reach the chemical transition state. Note that a 3′ dangling adenosine on the ribozyme near the hinge favors docking over coaxial stacking of the structural domains. (**C**) Fluorescence signals over time as a result of structure formation in the ribozyme–substrate complex. The double-labeled ribozyme displays a strong signal for the acceptor fluorophore and a weaker one for the donor. Upon manual addition of a 10-fold excess of non-cleavable substrate analog [S(dA$_{-1}$), with a deoxy modification at the scissile bond], significant quenching of the acceptor fluorescence is observed due to rapid ribozyme–substrate complex formation. Subsequently, the acceptor signal increases, while the donor signal decreases at the same rate. To analyze the data, a normalized ratio $Q$ of the acceptor:donor fluorescence as a measure for relative FRET efficiency was least-squares-fitted with the equation $y = y_0 + A(1–e^{-t/\tau})$, yielding a first-order reaction rate constant of $1/\tau = 0.61$ min$^{-1}$, with $A = 0.40$ and $\chi^2 = 0.00032$ (solid line). Conditions were 200 nM substrate and 20 nM hairpin ribozyme in 50 mM Tris–HCl, pH 7.5, 12 mM $MgCl_2$ and 25 mM DTT, at 25°C (standard buffer).

catalysis therefore appears to be to support folding of the RNA into a catalytically active structure, rather than a more direct function in reaction chemistry, such as activation of a bound water molecule as a general base catalyst or inner-sphere coordination to functional groups in the transition state (reviewed in Walter and Burke, 1998).

To better understand the molecular basis of catalysis by the hairpin ribozyme, we have been working to dissect its reaction pathway into individual steps (Figure 1B). In particular, it is very important to be able to monitor the interaction between the two domains in a manner that is independent of catalytic activity. The incorporation of fluorescent labels into specific sites of the ribozyme–substrate complex provides a spectroscopic tool to monitor the interactions between these sites, and to provide real-time information on structural changes. Turner *et al.* (1996) pioneered these methods for group I ribozymes. Previously, we have employed fluorescence quenching and dequenching assays to study the initial binding and dissociation of substrate analogs to the hairpin ribozyme (Walter and Burke, 1997; Walter *et al.*, 1997). Here we report the application of fluorescence resonance energy transfer (FRET) methods to elucidate the role of domain docking in the hairpin ribozyme reaction pathway. Our results demonstrate that a transition of the ribozyme–substrate complex from an open (undocked) into a closed (docked) form is a required step preceding substrate cleavage and ligation, and that docking is the rate-limiting step for product ligation. Multivalent metal ions are necessary for efficient docking of the two domains at low ionic strength and this may represent the predominant function of metal ions in catalysis.

## Results

### *Docking of the two domains of the ribozyme–substrate complex monitored by FRET*

To enable FRET measurements between domains A and B, we utilized a double-stranded version of the hairpin ribozyme which lacks a closing loop on helix 4 (Figure 1). This construct allows for synthesis of ribozyme and substrate by solid-phase synthesis (Chowrira and Burke, 1992) so that a 3′ fluorescein and a 5′ hexachlorofluorescein can be introduced as a donor–acceptor pair for FRET (Figure 1A). To ensure that all complexes contain donor and acceptor fluorophores in a 1:1 ratio, we coupled both fluorophores to the 5′ ribozyme segment. A 10-fold molar excess of the 3′ ribozyme segment was used to drive all of the fluorescently labeled strand into a complex. The sequence of both ribozyme and substrate are optimized for rapid substrate binding and efficient catalysis (Esteban *et al.*, 1997; Walter and Burke, 1997).

Previously, the reaction pathway of the hairpin ribozyme has been described as being composed of three major reversible steps: substrate binding; cleavage; and product dissociation (Hegg and Fedor, 1995; Esteban *et al.*, 1997; Walter and Burke, 1997). We suspected that a conformational change, docking of the two domains, occurred after binding and before the chemical steps of the reaction (Figure 1B). Our results clearly show that this is the case (Figure 1C).

Upon addition of a 10-fold excess of non-cleavable substrate analog S(dA$_{-1}$) to the double-labeled ribozyme under standard conditions (50 mM Tris–HCl, pH 7.5, 12 mM $MgCl_2$, 25 mM DTT as antioxidant, at 25°C), a rapid acceptor fluorescence decrease is observed which is completed within the time of manual mixing (~5 s; Figure 1C). Under these conditions, substrate binding is known to be very rapid ($k_{on}$ ~$2\times10^8$ $M^{-1}min^{-1}$, half-time 1.5 s; Esteban *et al.*, 1997; Walter and Burke, 1997). Because the fluorescence decrease was observed only with cognate substrate, we conclude that this rapid quenching is due to nucleobase-mediated quenching of hexachlorofluorescein in the ribozyme–substrate complex, presumably by a base-specific electron transfer mechanism involving the 3′-terminal uracils of the substrate (Walter and Burke, 1997).

Following substrate binding, changes of both donor and acceptor fluorescence occurred which are consistent with a decrease in the mean distance between the two fluorophores (Figure 1C). Figure 2 illustrates the changes in the ribozyme fluorescence emission spectrum before and after substrate addition. Since the donor and acceptor fluorophores are coupled to the ends of the two domains (Figure 1A), docking of the two domains can be expected to result in such an increase in transfer efficiency, with the donor becoming quenched and the acceptor emitting the transferred energy. Using tetramethylrhodamine as the acceptor gave very similar results. The changes in the ratio of acceptor:donor fluorescence provide a relative estimate for FRET efficiency (Table I). Fluorophore anisotropies were also measured; an increasing anisotropy of the acceptor fluorescence is indicative of decreasing fluorophore mobility upon substrate binding and complex docking (Table I).

The rate constant of the change in relative FRET efficiency in the presence of 10-fold excess of non-cleavable substrate analog was calculated from a single-exponential fit to the normalized acceptor:donor fluorescence ratio to yield $k_{dock,obs}$ = (0.64 ± 0.04) $min^{-1}$ (Figure 1C). Neither the rate constant nor the amplitude of the increase changed significantly as substrate analog concentration was increased by 10-fold [from 200 nM to 2 μM S(dA$_{-1}$); Table II], consistent with the underlying process being a tertiary structure transition in the ribozyme–substrate complex which is considerably slower than substrate binding. However, since the domain docking step has to be assumed to be reversible (and will be proven to be so), the observed docking rate constant $k_{dock,obs}$ is at least a combination of the elementary docking and undocking rate constants as identified in Figure 1B (Johnson, 1992):

$$k_{dock,obs} = k_{dock} + k_{undock} \quad (1)$$

If the FRET increase reflects more than a single reversible docking step, $k_{dock,obs}$ would be of an even more complex nature. For example, lowering the substrate concentration to 20 nM (to a 1:1 ratio with ribozyme) results in a decrease in $k_{dock,obs}$ (Table II) demonstrating that, at low substrate concentration, substrate binding contributes to the observed docking rate. For docking in the presence of cleavable substrate, the cleavage rate has to be considered. For the short substrates utilized in this study, product dissociation is very rapid (Hegg and Fedor, 1995; Esteban *et al.*, 1997). Therefore, cleavage can be regarded as irreversible and equation 1 is replaced with the following:

$$k_{dock,obs} = k_{dock} + k_{undock} + k_{cleav} \quad (2)$$

Interestingly, the fluorescence emission spectra of all hairpin ribozyme complexes with a flexible hinge between helices 2 and 3 are largely dominated by the acceptor peak (Figure 2). Fluorescein and hexachlorofluorescein are characterized by a Förster radius $R_0$ (the distance at

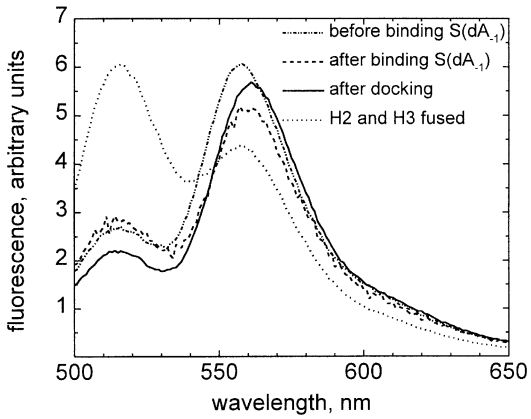


**Fig. 2.** Steady-state fluorescence emission spectra of 20 nM double-labeled hairpin ribozyme in standard reaction buffer. Spectra were taken before (dash-dotted line), immediately after (dashed line) manual addition of a 10-fold excess of non-cleavable substrate analog [S(dA$_{-1}$)] and after 20 min for complete tertiary structure formation of the ribozyme–substrate complex (solid line). Excitation was at 485 nm. The curves were obtained by averaging five spectra from the same solution. After addition of substrate analog, the acceptor fluorescence is quenched and its emission peak maximum is shifted slightly from 558 to 561 nm. In a construct where the 5′-end of the substrate is linked to the 3′-end of the ribozyme so that helices 2 and 3 of the ribozyme–substrate complex become fused, the spectrum is dominated by the donor emission peak at ~515 nm (dotted line).

**Table I.** Fluorescence properties of the double-labeled 5′ half of the hairpin ribozyme (5′Rz) before and after complex formation with the 3′ half (3′Rz) and the non-cleavable substrate analog S(dA$_{-1}$)[a]

| Molecules | Ratio of acceptor:donor fluorescence $Q = F_{560}/F_{515}$ | Acceptor anisotropy $A_{560}$[b] | Donor anisotropy $A_{515}$[c] |
|---|---|---|---|
| 20 nM 5′Rz | 5.5 ± 0.5 | 0.040 ± 0.002 | 0.15 ± 0.01 |
| 20 nM 5′Rz + 200 nM 3′Rz = 20 nM Rz | 2.1 ± 0.2 | 0.076 ± 0.002 | 0.13 ± 0.01 |
| 20 nM Rz + 200 nM S(dA$_{-1}$), before docking | 1.7 ± 0.1 | n.d.[d] | n.d.[d] |
| 20 nM Rz + 200 nM S(dA$_{-1}$), after docking | 2.4 ± 0.2 | 0.10 ± 0.01 | 0.13 ± 0.01 |
| 20 nM 5′Rz + 200 nM 3′Rz, covalently linked to S(dA$_{-1}$) | 0.7 ± 0.1 | 0.10 ± 0.01 | 0.074 ± 0.002 |

[a]All values were obtained in 50 mM Tris–HCl, pH 7.5, 12 mM $MgCl_2$, 25 mM DTT, at 25°C.
[b]Acceptor anisotropies were calculated from the mean of each 100 emission intensity values at 560 nm for the four different excitation and emission polarizer alignments using equation 4.
[c]Donor anisotropies were calculated from the mean of each 100 emission intensity values at 515 nm for the four different excitation and emission polarizer alignments using equation 4.
[d]n.d. = not determined.

**Table II.** Docking rate constants and relative amplitudes for modified complexes of substrate with double-labeled hairpin ribozyme as observed by an increase in their FRET signal[a]

| Substrate | Ribozyme[b] | Docking rate constant $k_{dock,obs}$ ($min^{-1}$) | Relative docking amplitude $A_{dock,rel}$[c] |
|---|---|---|---|
| 200 nM S(dA$_{-1}$) | 20 nM Rz(A$_{50}$) | 0.64 ± 0.04 | 1.00 ± 0.12 |
| 2 μM S(dA$_{-1}$) | 20 nM Rz(A$_{50}$) | 0.65 ± 0.04 | 1.07 ± 0.12 |
| 20 nM S(dA$_{-1}$) | 20 nM Rz(A$_{50}$) | 0.44 ± 0.04 | 0.91 ± 0.12 |
| 200 nM S | 20 nM Rz(A$_{50}$) | 1.02 ± 0.07 | 0.95 ± 0.20 |
| 1 μM S | 20 nM Rz(A$_{50}$) | 1.09 ± 0.07 | 0.88 ± 0.20 |
| 200 nM S(2′OMeA$_{-1}$) | 20 nM Rz(A$_{50}$) | 0.84 ± 0.04 | 0.86 ± 0.12 |
| 200 nM S(dA$_{-1}$) | 20 nM Rz(U$_{50}$) | 0.22 ± 0.02 | 0.42 ± 0.05 |
| 200 nM S | 20 nM Rz(U$_{50}$) | 0.38 ± 0.02 | 0.37 ± 0.05 |
| 200 nM S(2′OMeA$_{-1}$) | 20 nM Rz(U$_{50}$) | 0.33 ± 0.02 | 0.33 ± 0.05 |
| 200 nM S(dA$_{-1}$) | 20 nM Rz(Δ$_{50}$) | 0.20 ± 0.02 | 0.28 ± 0.03 |
| 200 nM S | 20 nM Rz(Δ$_{50}$) | 0.33 ± 0.02 | 0.21 ± 0.03 |
| 200 nM S(2′OMeA$_{-1}$) | 20 nM Rz(Δ$_{50}$) | 0.30 ± 0.02 | 0.08 ± 0.01 |
| 200 nM S(dA$_{-1}$) | 20 nM Rz(G$_{50}$) | 0.48 ± 0.04 | 0.98 ± 0.12 |
| 200 nM S(dA$_{-1}$) | 20 nM Rz(C$_{50}$) | 0.27 ± 0.04 | 0.70 ± 0.10 |
| 200 nM S(G$_{+1}$A) | 20 nM Rz(Δ$_{50}$) | – | 0 |
| 200 nM S(U$_{+2}$G,dA$_{-1}$) | 20 nM Rz(A$_{50}$) | 1.03 ± 0.06 (0.10 ± 0.02)[d] | 1.00 ± 0.07 (0.39± 0.05)[d] |
| 200 nM S(C$_{+3}$A,dA$_{-1}$) | 20 nM Rz(A$_{50}$) | 0.97 ± 0.05 | 0.77 ± 0.12 |
| 200 nM S(dA$_{-1}$) | 20 nM Rz(A$_{40}$G,U$_{42}$C,A$_{43}$G) | – | 0 |
| 200 nM S(dA$_{-1}$) | 20 nM Rz(dA$_9$,A$_{50}$) | 0.94 ± 0.05 | 1.05 ± 0.12 |
| 200 nM S(dA$_{-1}$) | 20 nM Rz(dA$_{10}$,A$_{50}$) | 1.91 ± 0.05 | 0.11 ± 0.05 |
| 200 nM S(dA$_{-1}$) | 20 nM Rz(dG$_{11}$,A$_{50}$) | 0.65 ± 0.20 | 0.05 ± 0.03 |

[a]Data analysis was as described in Materials and methods and as exemplified in Figure 1C; deviation ranges were obtained from at least two independent experiments; all values were measured in 50 mM Tris–HCl, pH 7.5, 12 mM $MgCl_2$, 25 mM DTT, at 25°C.
[b]Rz(A$_{50}$) is the standard hairpin ribozyme construct as described in Figure 1A; Rz(Δ$_{50}$) is lacking a nucleotide in position 50 (see Figure 1A).
[c]Docking amplitudes were normalized to the value for 200 nM S(dA$_{-1}$) in complex with 20 nM Rz(A$_{50}$).
[d]A double-exponential equation had to be used to accurately fit the data for substrate mutant S(U$_{+2}$G,dA$_{-1}$); the second phase values are given in parentheses.

which energy transfer is 50% efficient) of 4.4 nm. FRET efficiency decreases strongly with the fluorophore distance $r$ [proportional to $(R_o/r)^6$], and the length of an extended ribozyme–substrate complex as depicted in Figure 1B would be ~12 nm. Therefore, FRET efficiency for the complex is significantly higher than would be expected for a rigid molecule of that length (Wu and Brand, 1994). This was tested through the fusion of helices 2 and 3 by covalently linking the substrate 5′ and ribozyme 3′ ends, leading to the expected donor-dominated spectrum (Figure 2). Here, the remaining acceptor peak is mainly due to direct excitation. The high energy-transfer efficiency in all other ribozyme–substrate complexes supports the notion of a flexible and highly dynamic hinge between their domains A and B, so that the fluorophores can interact transiently even without domain docking.

### *Docking is required for substrate cleavage, but is not rate-limiting*

To study the significance of domain docking in the catalytic cycle, we used unmodified substrate to follow cleavage activity, as measured by a radioisotopic assay, together with conformational events, as measured by FRET (Figure 3A). Other work in our laboratory indicates that changes to the 3′ end of the ribozyme can increase stacking of helices 2 and 3, with a concomitant decrease in cleavage activity (Esteban *et al.*, 1998; J.E.Heckman, N.G.Walter, K.J.Hampel, E.K.O'Neill and J.M.Burke, in preparation).

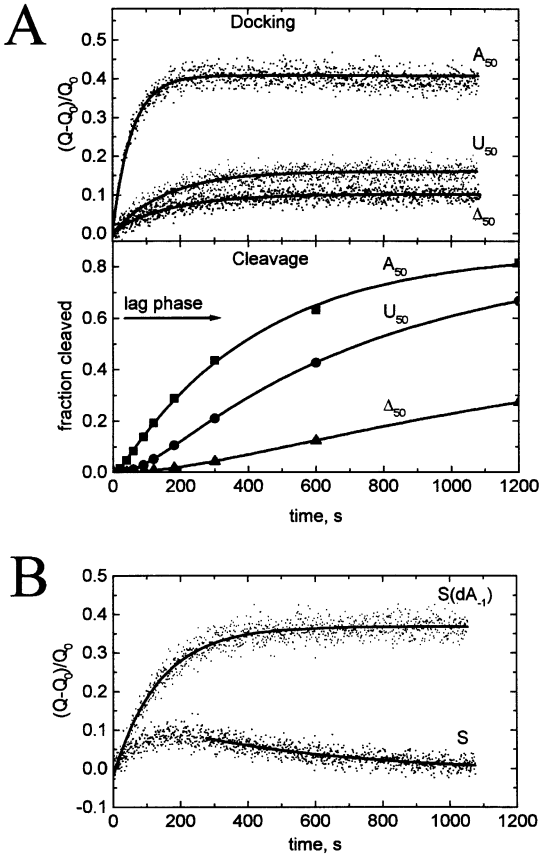


**Fig. 3.** Substrate docking precedes cleavage. (**A**) Upper panel: FRET increase after addition of 200 nM cleavable substrate to 20 nM ribozyme in standard buffer at 25°C. The data (1 datum $s^{-1}$) for three ribozymes with distinctive 3′ dangling overhangs ($A_{50}$, $U_{50}$ and $\Delta_{50}$) were least-squares-fitted to the equation $y = y_0 + A(1–e^{-t/\tau})$, yielding first order reaction rate constants of $1/\tau = 1.06$ $min^{-1}$ ($A = 0.40$, $\chi^2 = 0.00031$), $1/\tau = 0.38$ $min^{-1}$ ($A = 0.16$, $\chi^2 = 0.00024$) and $1/\tau = 0.34$ $min^{-1}$ ($A = 0.095$, $\chi^2 = 0.0002$), respectively (solid lines). Lower panel: radioactive cleavage assay with the same three double-stranded ribozymes without fluorophores under single-turnover conditions. Note that the occurrence of cleavage product is delayed by a lag phase of similar time frame as the occurrence of the FRET increase. The data could be fitted to the double-exponential equation $y = y_0 + A_1(1–e^{-t/\tau 1}) + A_2(1–e^{-t/\tau 2})$ with a 'fast' phase of negative amplitude $A_1$, which characterizes the lag, and a 'slower' second phase for the cleavage. Cleavage rate constants were 0.144 $min^{-1}$, 0.086 $min^{-1}$ and 0.024 $min^{-1}$ for the $A_{50}$, $U_{50}$ and $\Delta_{50}$ ribozymes, respectively. (**B**) FRET increase after addition of 20 nM of either cleavable substrate (S) or non-cleavable substrate analog [$S(dA_{-1})$] to 20 nM ribozyme in standard buffer at 25°C. The data (1 datum $s^{-1}$) for $S(dA_{-1})$ were fitted to the equation $y = y_0 + A(1–e^{-t/\tau})$ (solid line), yielding a first-order reaction rate constant of $1/\tau = 0.44$ $min^{-1}$ ($A = 0.39$, $\chi^2 = 0.00049$). The cleavable substrate displays an initial FRET increase that decreases again. The decrease (1 datum $s^{-1}$) was fitted to a single-exponential decay curve [$y = y_0 + A(e^{-t/\tau})$], yielding a rate constant of $1/\tau = 0.116$ $min^{-1}$ ($A = 0.09$, $\chi^2 = 0.00025$) (solid line).

Therefore, the unmodified hairpin ribozyme, containing a 3′-terminal adenosine at position 50, was analyzed along with two variants, containing a substitution ($U_{50}$) and a deletion ($\Delta_{50}$) at this position. The $U_{50}$ variant can potentially form a base pair with $A_{14}$ of the substrate-binding strand and, therefore, has a potential alternative extended conformation with a shifted stacking surface.

The unmodified ribozyme ($A_{50}$) displayed the fastest rate (1.06 $min^{-1}$) and greatest amplitude (0.40) of the FRET increase that accompanies docking (Figure 3A, upper panel). Each of the 3′-terminal modifications results in a significant decrease in both docking rate (0.38 $min^{-1}$ for $U_{50}$ and $k_{dock,obs}$ = 0.34 $min^{-1}$ for $\Delta_{50}$) and FRET amplitude (0.16 and 0.095, respectively). Cleavage rates (Figure 3A, lower panel) followed the same trend, with the rate constant for the $U_{50}$ variant (0.086 $min^{-1}$) intermediate between those of the unmodified $A_{50}$ (0.144 $min^{-1}$) and $\Delta_{50}$ (0.024 $min^{-1}$).

Comparison of the time courses of docking and cleavage clearly indicate that cleavage follows docking. Furthermore, the ribozyme reactions show a pronounced lag phase at the onset of cleavage, both with an excess of 100 nM (Figure 3A) and 1 μM ribozyme (data not shown). In each case, the FRET increase clearly precedes cleavage, demonstrating that the rate-limiting step for cleavage is an event that occurs after docking.

Docking rates and FRET amplitudes were not significantly altered when a 10- or 50-fold molar excess of cleavable substrate was present (Table II), indicating that steady-state conditions with a constant population of docked complexes are maintained. However, when an equimolar ratio of cleavable substrate to ribozyme was used, the FRET signal increased briefly and then started to decay with a rate corresponding to the cleavage rate (0.12 $min^{-1}$), indicating docking of uncleaved substrate and a subsequent undocking step following cleavage. This was confirmed by demonstrating that a non-cleavable substrate analog only showed a single-exponential increase in FRET signal under the same conditions (Figure 3B).

Together, these observations are consistent with the following model: (i) substrate docking rates are generally faster than those of cleavage so that docking precedes cleavage; (ii) the amplitude of FRET signal increase is proportional to the fraction of docked complexes, complexes in an undocked conformation do not contribute to the signal increase; (iii) docking is required prior to cleavage so that the higher the fraction of docked complexes, the faster the cleavage rate; and (iv) after cleavage, product dissociation is accompanied by relaxation into an undocked state.

These assumptions are reflected in the reaction scheme of Figure 1B, and are fully consistent with a computer simulation of the cleavage time courses based on this scheme, obtained using the program HopKINSIM 1.7.2. A unique solution to the time dependence of formation and decay of the docked intermediate (i.e. the solution to equation 2) could not be obtained from the available data, since this step requires an absolute measurement of the fraction of docked complexes (Johnson, 1992) and the nature of steady-state fluorescence measurements only provides relative values. However, by comparing cleavage activities of ribozyme variants with a different tendency to form inactive, coaxially stacked conformers (J.E.Heckman, N.G.Walter, K.J.Hampel, E.K.O'Neill and J.M.Burke, in preparation), we are able to estimate the fraction of active, docked complexes in the basic construct of Figure 1A to be ~65% under conditions of substrate excess. This value leads to estimates for $k_{dock}$ and $k_{undock}$ of 0.53 $min^{-1}$ and 0.32 $min^{-1}$, respectively. Substrate docking into an active ribozyme–substrate complex therefore is ~3.5 times faster than cleavage and shows significant reversibility.

### *Docking is required for ligation*

RNA molecules corresponding to the products of the cleavage reaction can be ligated very efficiently by the hairpin ribozyme (Buzayan *et al.*, 1986; Hegg and Fedor, 1995) with a rate constant for our construct of ~2.3 $min^{-1}$ (Esteban *et al.*, 1997). This rate is significantly greater than the observed rate of cleavage. To study the role of docking for this step without interference with reaction chemistry, we performed the FRET assay using 5′ product analogs with a phosphorylated or hydroxyl 3′ end. Ligation would require a 2′,3′-cyclic phosphate end at the reaction site. By adding either the 3′ or 5′ product analog first, we could show that the presence of both cleavage products is required for significant docking, i.e. FRET signal increase (Figure 4; Table III). The rate constant for docking involving the 3′ phosphorylated 5′ product (5′P) under standard conditions was 2.5 $min^{-1}$, a value remarkably close to the ligation rate constant. This value was similar for either 5 or 10 μM product concentration, demonstrating that the ribozyme is saturated with product strands under these conditions (Table III). However, docking in the presence of 5′ product with a 3′ hydroxyl end [5′P(3′OH)] appeared to be faster (3.8 $min^{-1}$) and to a lower FRET signal level (relative amplitude 0.28, compared with 0.51 for 5′P; Table III). When adding 5′P first, the higher FRET signal level decays to an intermediate value upon addition of 5′P(3′OH) (rate constant: 1.7 ± 0.3 $min^{-1}$; Figure 4). If 5′P(3′OH) is added first, the intermediate FRET signal level can be further increased by addition of phosphorylated 5′P (data not shown).

These findings are in accordance with the following notions. (i) The molecular recognition process between domains A and B requires elements located both upstream and downstream of the scissile bond, i.e. on both the 5′ and 3′ cleavage products. (ii) Ligation is accompanied by docking of the ribozyme–cleavage product complex; the observed ligation and docking rate constants are essentially identical. (iii) The fraction of docked complexes is higher if a phosphate on the 3′ end of the 5′ product is present; if both a 3′-phosphorylated and unphosphorylated 5′ product are added, they compete for formation of their respective docked complexes and reach equilibrium at a rate constant of ~1.7 $min^{-1}$. This observation implies that docking of the ribozyme–cleavage product complex is readily reversible, as proposed in the reaction mechanism of Figure 1B. Consequently, the faster rate of docking observed in the presence of 5′P(3′OH) (Table III) can be explained by a faster undocking rate than with 5′P (equation 1).

### *The magnesium dependency of docking rates, amplitudes and reaction rates for cleavage and ligation demonstrate that docking is rate-limiting for ligation, but not cleavage*

To determine whether docking is rate-limiting for either cleavage or ligation, we surveyed the $Mg^{2+}$-concentration dependence of docking rate constants and amplitudes together with cleavage rate constants (Figure 5). For cleavage, the shape of the $Mg^{2+}$-concentration dependence curve of catalysis closely parallels that describing the docking amplitude, reflecting the relative fraction of docked complexes (Figure 5A). Docking rates are higher than catalytic rates at all $Mg^{2+}$ concentrations, not only for the basic construct Rz($A_{50}$) of Figure 1A, but also for catalytically distinct variants such as Rz($U_{50}$) and Rz($\Delta_{50}$). These findings indicate that only docked complexes can perform catalysis, and that an additional step(s) after docking and before product-release limits the observed rate of reaction.

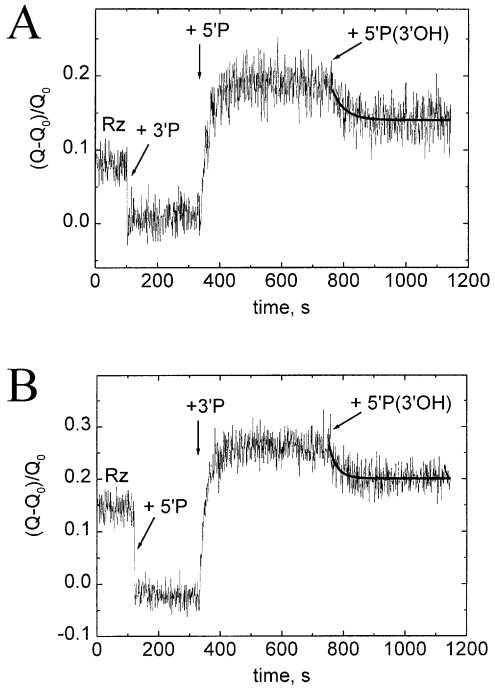


**Fig. 4.** Both 5′ and 3′ products are required for docking of the complex containing cleavage products. (**A**) To 20 nM double-labeled hairpin ribozyme (Rz) in standard buffer at 25°C, first an excess of 10 μM 3′ product (3′P) was added, then 10 μM 3′ phosphorylated 5′ product (5′P). Only after the second addition does the FRET signal increase (rate: 2.41 $min^{-1}$, amplitude: 0.19). Subsequent addition of an unphosphorylated 5′ product [5′P(3′OH)] results in a partial decrease in the FRET signal that could be fitted to a single-exponential decay curve [$y = y_0 + A(e^{-t/\tau})$], yielding a rate constant of $1/\tau$ = 1.43 $min^{-1}$ ($A$ = 0.06, $\chi^2$ = 0.00037) (thick line). (**B**) Complementary to the experiment in (A), first an excess of 10 μM 3′ phosphorylated 5′ product (5′P) was added to 20 nM double-labeled hairpin ribozyme (Rz), then 10 μM 3′ product (3′P). Only after the second addition does the FRET signal increase (rate: 2.68 $min^{-1}$, amplitude: 0.25). Subsequent addition of an unphosphorylated 5′ product [5′P(3′OH)] results in a partial decrease in the FRET signal that could be fitted to a single-exponential decay curve [$y = y_0 + A(e^{-t/\tau})$], yielding a rate constant of $1/\tau$ = 1.97 $min^{-1}$ ($A$ = 0.08, $\chi^2$ = 0.00036) (thick line).

For ligation, the situation is different. The $Mg^{2+}$-concentration dependence of the ligation rate constant closely follows that for the docking rate constant (Figure 5B). Their values are in good agreement at all $Mg^{2+}$ concentrations. Thus, docking is both required and rate-limiting for ligation, so that a ligation rate constant of 2.3 $min^{-1}$ under standard conditions (50 mM Tris–HCl, pH 7.5, 12 mM $MgCl_2$, at 25°C) monitors product docking. By contrast, the docking amplitude or relative fraction of docked complexes quickly levels off with increasing $Mg^{2+}$ concentration. Since the fraction of docked complexes is dependent on the ratio of the two rate constants $k_{dock}$ and $k_{undock}$, and since $k_{dock,obs} = k_{dock} + k_{undock}$ (equation 1), both docking and undocking rate constants must increase with [$Mg^{2+}$] in a way that maintains a constant fraction of docked complex.

**Table III.** Docking rates and relative amplitudes for complexes of 5′ and 3′ cleavage product analogs with double-labeled hairpin ribozyme as observed by an increase in their FRET signal[a]

| Cleavage product analogs | Docking rate constant $k_{dock,obs}$ ($min^{-1}$) | Relative docking amplitude $A_{dock,rel}$[b] |
|---|---|---|
| 10 μM 5′P | - | 0 |
| 10 μM 5′P(3′OH) | - | 0 |
| 10 μM 3′P | - | 0 |
| 10 μM 5′P + 10 μM 3′P | 2.47 ± 0.22 | 0.51 ± 0.07 |
| 5 μM 5′P + 5 μM 3′P | 2.10 ± 0.30 | 0.51 ± 0.07 |
| 10 μM 5′P(3′OH) + 10 μM 3′P | 3.77 ± 0.80 | 0.28 ± 0.07 |

[a]Data analysis was as described in Materials and methods and as exemplified in Figure 1C; deviation ranges were obtained from at least two independent experiments; all values were measured with 20 nM standard ribozyme (see Figure 1A) in 50 mM Tris–HCl, pH 7.5, 12 mM $MgCl_2$, 25 mM DTT, at 25°C; the 5′ product analogs were non-ligatable since they contained a 3′ phosphate (5′P) or a 3′ hydroxyl [5′P(3′OH)].
[b]Docking amplitudes were normalized to the value for 200 nM S($dA_{-1}$).

### *Docking and reactivity have essentially identical requirements for sequence, pH and temperature*

Docking of domains A and B of the hairpin ribozyme–substrate complex was studied by introducing substrate modifications near the scissile bond. First, alterations to the 2′ hydroxyl group at the cleavage site were investigated. For all three ribozyme variants ($A_{50}$, $U_{50}$ and $\Delta_{50}$), docking rate constants for the unmodified substrate S were highest (1.02 $min^{-1}$, 0.38 $min^{-1}$ and 0.33 $min^{-1}$, respectively), while those for a 2′ *O*-methylated substrate S(2′OMe$A_{-1}$) were intermediate (0.84 $min^{-1}$, 0.33 $min^{-1}$ and 0.30 $min^{-1}$, respectively), and those of the 2′-deoxy modified substrate S($dA_{-1}$) were lowest (0.64 $min^{-1}$, 0.22 $min^{-1}$, 0.20 $min^{-1}$, respectively). Differences between the docking rate constants for the unmodified substrate and its *O*-methylated analog are closely correlated with cleavage rate constants for the three ribozyme variants (0.144 $min^{-1}$, 0.086 $min^{-1}$ and 0.024 $min^{-1}$, respectively; Figure 3A), in accordance with equations 2 (cleavable substrate) and 1 (2′OMe$A_{-1}$ substrate). The 2′ *O*-methylated substrate appears to be the best mimic of the unmodified substrate, and therefore is the analog of choice for probing the tertiary structure of the active ribozyme–substrate complex. The deoxy $A_{-1}$ substrate analog forms docked complexes with the ribozyme, but the reduction in the observed docking rate beyond that expected from blocking cleavage indicates that this modification results in a slight destabilization or other change in the tertiary structure of the docked complex.

### *Essential substrate base $G_{+1}$ is required for formation of the docked complex*

Substrate base substitutions near the cleavage site have been identified that significantly inhibit cleavage. Do they inhibit the reaction by inhibiting docking, or do they act on an essential step that follows formation of the docked complex? Previously, we showed that substitution of the guanosine immediately 3′ of the cleavage site with A, C or U resulted in profound inhibition of the reaction (Chowrira *et al.*, 1991). Use of the $G_{+1}A$ variant in the FRET assay shows that the modified substrate binds to the substrate-binding strand, as indicated by quenching of the ribozyme's 5′ fluorophore. However, no subsequent increase in fluorescence was observed (Figure 6; Table II), even when magnesium ion concentrations as high as 200 mM were employed. Therefore, we conclude that the mechanism of inhibition by the $G_{+1}A$ substitution involves blocking the required docking of the two domains.

For a substrate variant with a $U_{+2}G$ change, cleavage activity is decreased 4-fold (Chowrira *et al.*, 1991), but domain docking remains efficient (Table II). However, the FRET signal increase clearly displays a second, slower phase; a unique feature among all tested modifications of sequence or conditions (Figure 6). It is possible that this second phase reflects an additional structural change in the ribozyme–substrate complex that occurs after the initial domain docking event. This additional step may well be associated with the decreased rate of cleavage. A substrate variation $C_{+3}A$ decreases cleavage activity on the substrate 5-fold (Chowrira *et al.*, 1991). However, the observed docking rate constant (0.97 $min^{-1}$) is comparable with that of the unmodified substrate with only a slightly decreased (23%) docking amplitude (Figure 6; Table II).

### *Modifications to the ribozyme inhibit docking*

Internal loop B of the ribozyme contains a number of highly conserved bases (reviewed in Burke *et al.*, 1996), especially within a UV-cross-linkable tertiary structure motif adjacent to helix 3 which is critical for catalytic activity (Butcher and Burke, 1994). Disabling this motif by mutating three of the conserved bases ($A_{40}G$, $U_{42}C$ and $A_{43}G$) completely abolishes catalytic activity. We found the reason to be interference with domain docking, as demonstrated by a lack of FRET signal increase (Table II).

Four ribose 2′ hydroxyl groups in the hairpin ribozyme have been shown to be important for catalytic activity; two are located in domain A (positions 10 and 11) and two lie within domain B (positions 24 and 25) (Chowrira *et al.*, 1993b). Recently, these four hydroxyl groups have been proposed to form an important component of the interdomain interaction through formation of a ribose zipper (Earnshaw *et al.*, 1997). To analyze their relevance for domain docking experimentally, we introduced 2′ deoxy modifications to three ribose moieties of the double-labeled ribozyme. Deletion of the 2′-OH groups of $A_{10}$ and $G_{11}$ severely interferes with docking of domains, while an analogous modification at a non-essential site ($dA_9$) had no effect on docking (Figure 7; Table II). The residual docking activity with the two ribozyme variants Rz($dA_{10}$) and Rz($dG_{11}$) is enhanced by increasing the $Mg^{2+}$ concentration to 50 mM (data not shown), as is catalytic activity for Rz($dG_{11}$) (Chowrira *et al.*, 1993b).

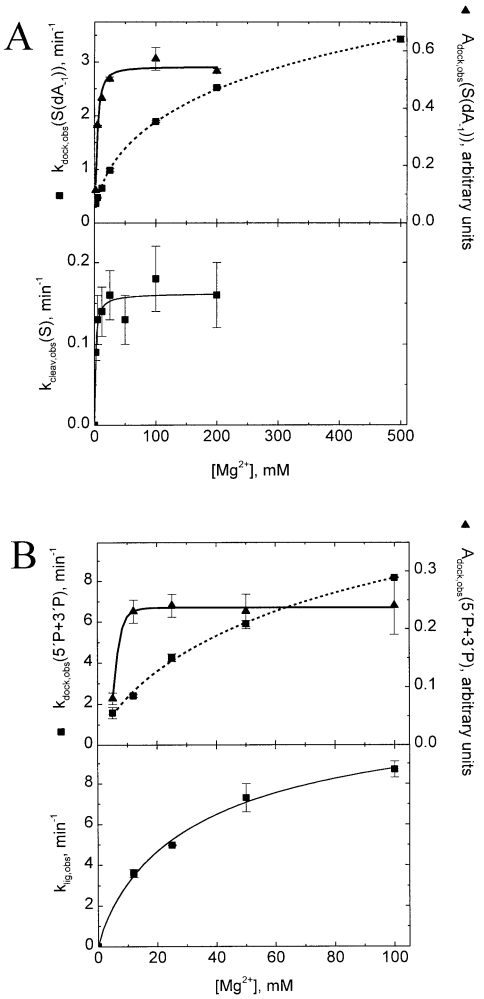


**Fig. 5.** Magnesium ion-dependence of docking, cleavage and ligation. (**A**) Upper panel: the $Mg^{2+}$-concentration dependence of domain docking rate constant (squares) and amplitude (triangles) for the complex of hairpin ribozyme with non-cleavable substrate analog S(dA$_{-1}$) were fitted to cooperativity equation 3 as described in Materials and methods, yielding $K_D^{Mg}$ = 1100 mM, $n$ = 0.54 (solid line) and $K_D^{Mg}$ = 4.14 mM, $n$ = 1.6 (dashed line), respectively. Lower panel: the $Mg^{2+}$-concentration dependence of substrate cleavage by an unlabeled two-strand hairpin ribozyme were fitted to equation 3 as above, yielding $K_D^{Mg}$ = 1.5 mM, $n$ = 0.98 (solid line). (**B**) Upper panel: the $Mg^{2+}$-concentration dependence of domain docking rate constant (squares) and amplitude (triangles) for the complex of hairpin ribozyme with 5′ and 3′ products (5′P and 3′P) were fitted to cooperativity equation 3 as described in Materials and methods, yielding $K_D^{Mg}$ = 130 mM, $n$ = 0.75 (solid line) and $K_D^{Mg}$ = 5.7 mM, $n$ = 4.8 (dashed line), respectively. Lower panel: the $Mg^{2+}$-concentration dependence of product ligation by an unlabeled one-strand hairpin ribozyme (with a closing loop on helix 4; Figure 1A) were fitted to equation 3 as above, yielding $K_D^{Mg}$ = 36 mM, $n$ = 0.86 (solid line). Ligation rate data are taken from A.R.Banerjee, J.A.Esteban and J.M.Burke (in preparation).

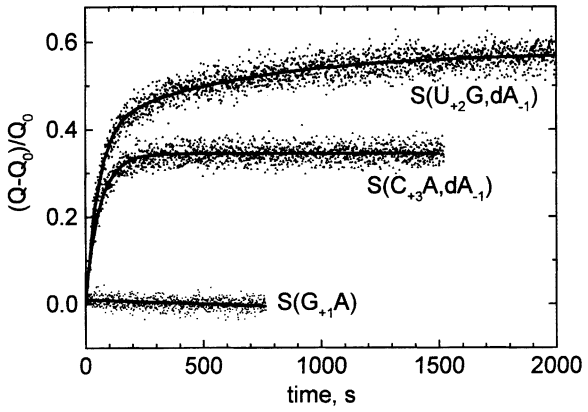


**Fig. 6.** Docking of complexes between hairpin ribozyme and substrate variants. The FRET signal change after addition of 200 nM of substrate variants S(G$_{+1}$A), S(U$_{+2}$G,dA$_{-1}$) and S(C$_{+3}$A,dA$_{-1}$) to 20 nM ribozyme was monitored in standard buffer at 25°C. The FRET signal for S(G$_{+1}$A) did not increase over time. Changing U$_{+2}$ in S(U$_{+2}$G,dA$_{-1}$) resulted in a double-exponential FRET increase that was fitted to the equation $y = y_0 + A_1(1-e^{-t/\tau 1}) + A_2(1-e^{-t/\tau 2})$, yielding rate constants of $1/\tau_1$ = 1.08 min$^{-1}$ ($A_1$ = 0.41) and $1/\tau_2$ = 0.09 min$^{-1}$ ($A_2$ = 0.17, $\chi^2$ = 0.00045) (solid line). The FRET signal for S(C$_{+3}$A,dA$_{-1}$) could be fitted to the single-exponential equation $y = y_0 + A(1-e^{-t/\tau})$ with $1/\tau$ = 0.97 min$^{-1}$ ($A$ = 0.33, $\chi^2$ = 0.00031) (solid line).

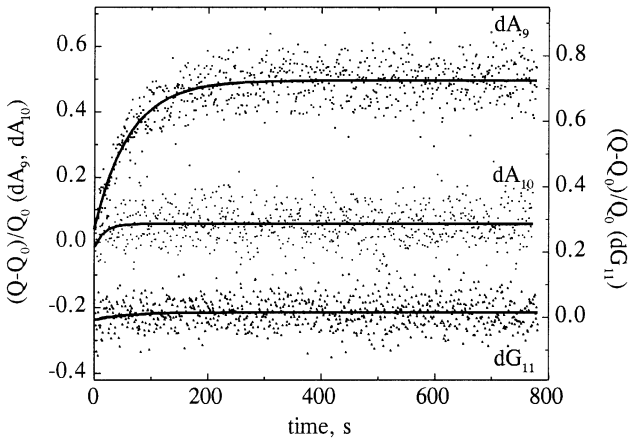


**Fig. 7.** Docking of complexes with deoxy modifications in the ribozyme part of domain A. The FRET signal change after addition of 200 nM of substrate S(dA$_{-1}$) to 20 nM modified ribozyme was monitored in standard buffer at 25°C. The FRET signals of ribozymes with deoxy modifications in position 10 and 11 (dA$_{10}$ and dG$_{11}$) increased only slightly over time. As a positive control, a non-critical deoxy modification in position 9 (dA$_9$) yielded a FRET signal increase that was fitted to the equation $y = y_0 + A(1-e^{-t/\tau})$ with $1/\tau$ = 0.98 min$^{-1}$ ($A$ = 0.45, $\chi^2$ = 0.00036) (solid line).

Hairpin ribozyme cleavage is thought to follow a reaction pathway involving deprotonation of the 2′ hydroxyl group at the cleavage site and nucleophilic attack of the 2′ oxygen on the 3′ phosphate, a step expected to be highly pH-dependent (reviewed in Long and Uhlenbeck, 1993). However, both cleavage and ligation reaction rate constants were found to have a shallow pH dependence, their rates changing <5-fold between pH 5 and 10 (Nesbitt *et al.*, 1997; A.R.Banerjee, J.A.Esteban and J.M.Burke, in preparation). Notably, we found the pH-dependence of substrate-mediated domain docking to be low throughout the experimentally accessible range of pH 6.5–9.0 (Figure 8A; Table IV). While docking is not rate-limiting for substrate cleavage, this finding could explain the pH-independence of ligation, as the observed ligation rate monitors docking of the ribozyme–cleavage product complex as its rate-limiting step. That is, the pH-independence of ligation may be explained by a rate-determining and pH-independent docking step that masks pH-sensitive cleavage chemistry.

Domain docking in the presence of substrate was found to be strongly temperature-dependent. In fact, an activation energy of 28.8 kcal/mol was deduced from an Arrhenius

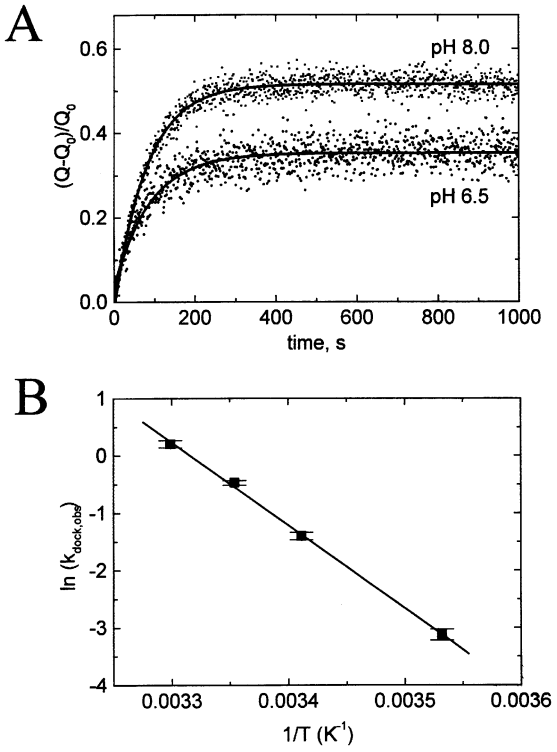


**Fig. 8.** pH and temperature dependence of docking. (**A**) FRET signal change after addition of 200 nM of substrate S(dA$_{-1}$) to 20 nM ribozyme in either 50 mM Tris–HCl, pH 8.0, or 50 mM MES–NaOH, pH 6.5 (both in the presence of 12 mM $MgCl_2$, 25 mM DTT), at 25°C. The data were fitted to the equation $y = y_0 + A(1–e^{-t/\tau})$ (solid lines), yielding first-order reaction rate constants of $1/\tau = 0.74$ min$^{-1}$ (pH 8.0; $A = 0.53$, $\chi^2 = 0.00043$) and $1/\tau = 0.67$ min$^{-1}$ (pH 6.5; $A = 0.32$, $\chi^2 = 0.00095$), respectively. (**B**) The observed docking rate constants from the FRET signal increase after addition of 200 nM of substrate S(dA$_{-1}$) to 20 nM ribozyme in standard reaction buffer (50 mM Tris–HCl, pH 7.5, 12 mM $MgCl_2$, 25 mM DTT) at different temperatures were used to obtain an Arrhenius plot. The observed activation energy was 28.8 ± 0.9 kcal/mol.

plot of docking rate constants (Figure 8B). This value is close to the activation energy for the cleavage reaction of 19–22 kcal/mol (Hampel and Tritz, 1989; A.R.Banerjee, J.A.Esteban and J.M.Burke, in preparation). However, since domain docking is not rate-limiting for cleavage, this similarity may well be coincidental.

### *Efficient domain docking requires multivalent metal ions*

The observation that a modest level of catalytic activity could be obtained in spermidine plus metal chelating agents (Chowrira *et al.*, 1993), together with recent findings that cobalt (III) hexammine supports catalysis (Hampel and Cowan, 1997; Nesbitt *et al.*, 1997; Young *et al.*, 1997) and that an efficient reaction proceeds in high concentrations of monovalent metal ions (J.B.Murray, A.A.Seyhan, J.M.Burke and W.G.Scott, in preparation) strongly argue against direct participation of metal ions in the catalytic mechanism. Thus, they function neither through activation of a bound water molecule as a general base catalyst nor by stabilizing a developing negative charge in the transition state, acting as a Lewis acid catalyst. Since metal ions traditionally have been thought to be intricately involved in RNA catalysis, these findings have raised the question of their role in hairpin ribozyme activity (reviewed in Walter and Burke, 1998).

We tested the ability of a variety of cations to facilitate assembly of the docked complex. In general, there is a striking similarity between ionic requirements for cleavage and docking; for example, divalent metal ions such as $Mg^{2+}$, $Ca^{2+}$ and $Sr^{2+}$ have been shown to result in substrate cleavage by the hairpin ribozyme and also lead to efficient docking (Table IV). For $Ca^{2+}$ and $Sr^{2+}$, a threshold concentration of ~5 mM must be exceeded to lead to significant cleavage (Chowrira *et al.*, 1993a), and the same is true for domain docking (Table IV). In the presence of 12 mM $Mg^{2+}$, spermidine induces a modest reduction in both docking rate and amplitude (Figure 9A; Table IV), consistent with its effect on cleavage activity (Chowrira *et al.*, 1993a). Alone, spermidine can promote neither an efficient cleavage reaction nor domain docking (Figure 9B; Table IV).

This combination of magnesium and spermidine permits us to investigate the reversibility of the docking step. Following the assembly of a docked complex, EDTA was used to chelate the magnesium, while spermidine served to stabilize the secondary structure of the complex between the three RNA strands. A rapid decay of the FRET signal ensued, resulting from undocking of the complex (Figure 9A). We estimate a lower limit of the undocking rate of 3.1 min$^{-1}$.

At low concentrations (2 mM) of either $Mg^{2+}$ or $Mn^{2+}$, spermidine enhances the rate of cleavage (Chowrira *et al.*, 1993a), and again similar effects are observed on docking rates and amplitudes (Figure 9B; Table IV). This finding suggests that low concentrations of spermidine, although incapable of promoting efficient docking, can stabilize important docking interactions when divalent metal ions are present.

Our ability to obtain information on the activity of cobalt (III) hexammine in docking was limited by quenching of the fluorescence signals by $[Co(NH_3)_6]^{3+}$. However, a fast docking step in the presence of $[Co(NH_3)_6]^{3+}$ and its enhancement by addition of 100 mM NaCl could be observed using the FRET-based assay (Table IV). Activity in the presence of $[Co(NH_3)_6]^{3+}$ is enhanced by addition of 100 mM NaCl (Hampel and Cowan, 1997). Finally, monovalent cations such as $Li^+$, $Na^+$, $K^+$ and $NH_4^+$ in concentrations up to 200 mM do not promote cleavage activity (Chowrira *et al.*, 1993a), consistent with their inability to promote significant domain docking (Table IV).

## Discussion

FRET has previously been utilized to follow hybridization kinetics of DNA strands (Morrison and Stols, 1993; Yang *et al.*, 1994; Parkhurst and Parkhurst, 1995) and, in the case of the hammerhead ribozyme, to measure distances (Tuschl *et al.*, 1994; Bassi *et al.*, 1997) and follow cleavage kinetics (Perkins *et al.*, 1996). In this paper, we demonstrate that FRET can be a very valuable tool for analysis of tertiary structure and associated dynamics in the hairpin ribozyme, by following changes in the proximity of the two structural domains, each labeled with one part of a fluorescence donor–acceptor pair. By measuring rates and amplitudes of the increase in FRET signal associated with docking, docking rates can be measured with high

**Table IV.** Docking rate constants and relative amplitudes for complexes of 200 nM substrate analog S(dA$_{-1}$) with 20 nM double-labeled hairpin ribozyme in different buffers as observed by an increase in FRET signal[a]

| Buffer conditions | Docking rate constant $k_{dock,obs}$ ($min^{-1}$) | Relative docking amplitude $A_{dock,rel}$[b] |
|---|---|---|
| 2 mM $Mg^{2+}$, pH 7.5 | 0.36 ± 0.03 | 0.26 ± 0.06 |
| 12 mM $Mg^{2+}$, pH 7.5 | 0.64 ± 0.04 | 1.00 ± 0.12 |
| 50 mM $Mg^{2+}$, pH 7.5 | 1.42 ± 0.05 | 1.10 ± 0.12 |
| 2 mM $Ca^{2+}$, pH 7.5 | – | 0 |
| 12 mM $Ca^{2+}$, pH 7.5 | 1.79 ± 0.10 | 0.54 ± 0.08 |
| 50 mM $Ca^{2+}$, pH 7.5 | 3.67 ± 0.25 | 0.55 ± 0.08 |
| 2 mM $Sr^{2+}$, pH 7.5 | – | 0 |
| 12 mM $Sr^{2+}$, pH 7.5 | 1.74 ± 0.10 | 0.25 ± 0.06 |
| 50 mM $Sr^{2+}$, pH 7.5 | 2.02 ± 0.15 | 0.49 ± 0.08 |
| 2 mM $Mn^{2+}$, pH 7.5 | 0.69 ± 0.04 | 0.38 ± 0.07 |
| 12 mM $Mn^{2+}$, pH 7.5 | 1.02 ± 0.05 | 0.63 ± 0.12 |
| 2 mM $Mn^{2+}$, 10 mM $spd^{+++}$, pH 7.5 | 0.51 ± 0.04 | 0.93 ± 0.12 |
| 2 mM $Mg^{2+}$, 2 mM $spd^{+++}$, pH 7.5 | 0.71 ± 0.05 | 0.16 ± 0.04 |
| 2 mM $Mg^{2+}$, 10 mM $spd^{+++}$, pH 7.5 | 1.30 ± 0.07 | 0.12 ± 0.03 |
| 12 mM $Mg^{2+}$, 10 mM $spd^{+++}$, pH 7.5 | 0.54 ± 0.04 | 0.95 ± 0.12 |
| 10 mM $[Co(NH_3)_6]^{3+}$, pH 7.5 | 1.54 ± 0.35 | 0.21 ± 0.05 |
| 10 mM $[Co(NH_3)_6]^{3+}$, 100 mM NaCl, pH 7.5 | 4.4 ± 1.0 | 0.43 ± 0.08 |
| 10 mM $spd^{+++}$, 2 mM EDTA, pH 7.5 | – | 0 |
| 100 mM $Li^{+}$, pH 7.5 | – | 0 |
| 200 mM $Na^{+}$, 2 mM EDTA, pH 7.5 | – | 0 |
| 200 mM $K^{+}$, pH 7.5 | – | 0 |
| 200 mM $NH_4^{+}$, pH 7.5 | – | 0 |
| 12 mM $Mg^{2+}$, pH 9.0 | 0.49 ± 0.04 | 0.77 ± 0.10 |
| 12 mM $Mg^{2+}$, pH 8.0 | 0.74 ± 0.05 | 1.23 ± 0.16 |
| 12 mM $Mg^{2+}$, pH 7.0 | 0.74 ± 0.04 | 0.49 ± 0.10 |
| 12 mM $Mg^{2+}$, pH 6.5 | 0.67 ± 0.04 | 0.74 ± 0.12 |

[a]Data analysis was as described in Materials and methods and as exemplified in Figure 1C; deviation ranges were obtained from at least two independent experiments; all values were measured at 25°C and in the presence of 25 mM DTT [except the cobalt (III) hexammine containing buffers, where addition of DTT resulted in a precipitant].
[b]Docking amplitudes were normalized to the value in 12 mM $Mg^{2+}$, pH 7.5.

precision and the extent of docking could be estimated. The rate constants that we observe for docking, 0.5 $min^{-1}$ for the substrate-bound complex and 2 $min^{-1}$ for the complex containing bound cleavage products, are similar to those measured for global folding events in more complex RNA molecules (Draper, 1996).

Our results support the following model of structural events during the cleavage reaction catalyzed by the hairpin ribozyme. An initial interaction occurs between substrate and ribozyme with formation of an undocked configuration, in which the molecule has access to an extended configuration characterized by coaxial stacking of helices 2 and 3 (this work; Esteban *et al*., 1998). After substrate binding, the dynamic flexibility about the hinge between helices 2 and 3 is utilized to explore possible contact modes between internal loops A and B of the two domains, leading finally to metastable, reversible docking of the two domains in a docked or 'closed' conformation which is an essential intermediate on the folding pathway leading to catalysis (Figure 1B). We have shown previously that substrate binding is essentially irreversible (Esteban *et al.*, 1997), so the substrate is expected to remain bound during the time required for formation of the closed complex. The highly reversible cleavage step is then followed by product dissociation and undocking. Because the dissociation of cleavage products is very rapid (Esteban *et al.*, 1997), it is likely that dissociation and undocking are a concerted process.

What do our results tell us about the catalytic mechanism of the ribozyme? Previous investigations of the hairpin ribozyme have served to identify a number of components that stimulate catalytic activity strongly, including metal ions {particularly $Mg^{2+}$ and $[Co(NH_3)_6]^{3+}$}, the cleavage site guanosine, 2′ hydroxyl groups within the ribozyme and at the scissile bond, and a conserved tertiary structure motif within internal loop B. Perhaps the most striking conclusion from the work presented here is that with a single exception, all of these components and conditions are essential for formation of the closed complex. The only modification that we have identified that permits formation of the closed complex without proceeding to cleavage is the modification of the 2′-OH group in the substrate, which functions intimately in the reaction chemistry as the attacking nucleophile. Although it remains possible that one or more of the components essential for docking could also play a role in reaction chemistry or other essential processes after docking and before cleavage, our results show that there is no need to assume that this is the case. They also provide a direct demonstration that base substitutions, RNA modifications or metal ions which inhibit ribozyme reactions at a step after substrate binding are not necessarily involved in catalysis.

Studies of reaction chemistry require the identification of the rate-limiting step and the ability to isolate experimentally the chemical step of the reaction pathway. Our results show that docking is rate-limiting for the ligation reaction, under conditions where domain A is fully occupied by the ligation substrates (cleavage products). Therefore, the ligation rate must exceed the docking rate, which is 2 $min^{-1}$ under standard conditions. Analysis of the chemistry of the ligation reaction will require the identification of reaction conditions, or manipulating the

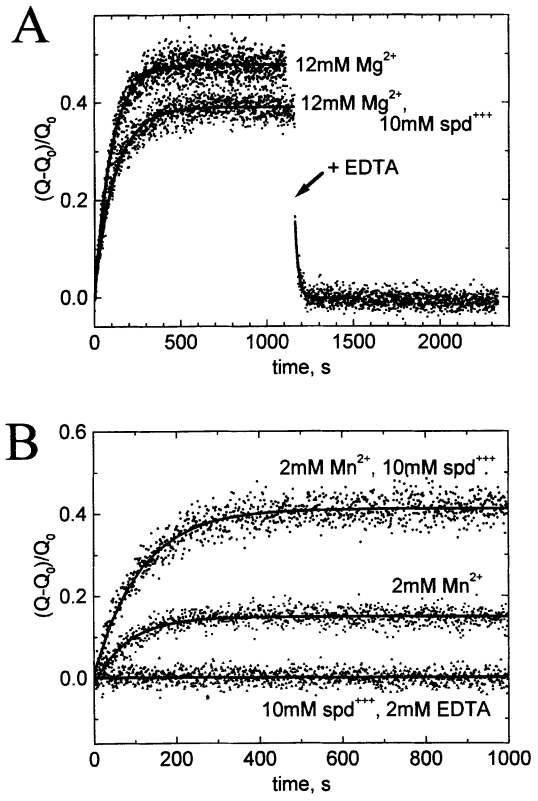


**Fig. 9.** Docking of hairpin-ribozyme–substrate complexes in the presence of different cations. (**A**) FRET signal increase after addition of 200 nM of substrate S(dA$_{-1}$) to 20 nM ribozyme in standard buffer at 25°C, compared with the increase in the same buffer with 10 mM spermidine ($spd^{+++}$) added. The FRET signal in 12 mM $Mg^{2+}$ could be fitted to the equation $y = y_0 + A(1–e^{-t/\tau})$ with $1/\tau = 0.63$ min$^{-1}$ ($A = 0.48$, $\chi^2 = 0.00048$) (solid line), while the data from 12 mM $Mg^{2+}$, 10 mM $spd^{+++}$ yielded $1/\tau = 0.50$ min$^{-1}$ ($A = 0.37$, $\chi^2 = 0.0004$) (solid line). To the latter reaction mixture, 25 mM EDTA were added to chelate $Mg^{2+}$, resulting in undocking of the docked ribozyme–substrate complex. This effect was monitored by a fast single-exponential FRET signal decrease, that was fitted to the equation $[y = y_0 + A(e^{-t/\tau})]$ to yield a lower-limit rate constant of $1/\tau = 3.1$ min$^{-1}$ ($\chi^2 = 0.00019$) (solid line). (**B**) Changes in FRET signal after addition of 200 nM of substrate S(dA$_{-1}$) to 20 nM ribozyme in 50 mM Tris–HCl, pH 7.5, 12 mM $MgCl_2$, 25 mM DTT, at 25°C, with either 10 mM $spd^{+++}$ and 2 mM EDTA, or 2 mM $Mn^{2+}$, or 2 mM $Mn^{2+}$ and 10 mM $spd^{+++}$ added. Spermidine alone did not result in significant docking after formation of the ribozyme–substrate complex. The data for 2 mM $Mn^{2+}$ were fitted to the equation $y = y_0 + A(1–e^{-t/\tau})$ with $1/\tau = 0.74$ min$^{-1}$ ($A = 0.16$, $\chi^2 = 0.00029$) (solid line), while the data for 2 mM $Mn^{2+}$, 10 mM $spd^{+++}$ yielded $1/\tau = 0.51$ min$^{-1}$ ($A = 0.40$, $\chi^2 = 0.00073$) (solid line).

structure of the RNA in such a way that a reaction can be initiated from a pre-docked complex.

In the case of the cleavage reaction, docking is significantly faster than cleavage under all conditions analyzed, and so is not the rate-limiting step. Parallel time courses of docking and cleavage (Figure 3A) show that cleavage always lags behind formation of the docked complex. At least two models could account for this behavior. First, the observed cleavage rates could be a direct measurement of a slow chemical step. Alternatively, an additional and rate-limiting step could occur after the docking event measured by FRET and before the cleavage reaction. In light of the very surprising pH- and metal ion-independence of the reaction, we favor the second model and believe that a rate-limiting conformational change after docking may be the most plausible hypothesis.

The sequence, pH, temperature and ionic requirements for docking are in very close agreement with previously identified requirements for catalytic activity, which is evidence of the importance of docking for catalytic activity. Indeed, we were able to demonstrate that docking is a necessary step prior to cleavage, and that it is both essential and rate-limiting for ligation.

The observation that metal ions {$Mg^{2+}$, $Ca^{2+}$, $Sr^{2+}$, $Mn^{2+}$ or $[Co(NH_3)_6]^{3+}$} are required for docking provides an explanation for their role in the catalytic mechanism. Because the kinetically inert cobalt (III) hexammine complex promotes an efficient cleavage reaction, doubts have recently been raised that metal ions play an active role in the reaction pathway; for example, by providing a bound water molecule as general base catalyst or by stabilizing negative charges in the transition state (Hampel and Cowan, 1997; Nesbitt *et al.*, 1997; Young *et al.*, 1997). However, their role might rather be to stabilize a catalytically active tertiary structure like the docked ribozyme–substrate complex observed by FRET. With other cations, such as spermidine or $Na^+$, no docking has been observed. They lead to catalytic activity only at very high concentrations (Hampel and Cowan, 1997; J.B.Murray, A.A.Seyhan, J.M.Burke and W.G.Scott, in preparation), suggesting that docking is unfavorable unless the repulsive negative backbone charges of the approaching RNA domains are completely shielded.

The data presented here are consistent with a recently proposed tertiary structure model of the hairpin ribozyme (Earnshaw *et al.*, 1997). Here, the 2′ hydroxyl groups of residues $A_{10}$ and $G_{11}$ of domain A, and $A_{24}$ and $C_{25}$ of domain B, connect the two domains through hydrogen bonding in a ribose ‘zipper’. We found the hydroxyls of $A_{10}$ and $G_{11}$ to be intimately involved in domain docking, since deoxy modifications in these sites severely impaired docking activity in the FRET assay. The FRET experiments, however, provide no information about whether the hydroxyls of $A_{10}$ and $G_{11}$ interact with those of $A_{24}$ and $C_{25}$, or with some other part of the closed complex. Our data suggest that the docked complex is stabilized by a network of weak interactions in such a way that disruption of any of a number of interactions prevents docking. In addition, our results show that other components are clearly of equal importance to docking of the two domains, since base changes in positions +1 and +2 of the substrate, a deoxy modification in its –1 position and the lack of a 3′ phosphate in the 5′ product all influence the rate of docking. Contact points between the two domains as well as the sequence and cation requirements for docking have been studied recently by chemical footprinting (K.J.Hampel, N.G.Walter and J.M.Burke, in preparation). Multivalent metal ions appear to play a crucial role in docking under conditions of low monovalent cation concentration, possibly by bridging negative charges at the interface between domains.

The kinetic pathways of RNA folding have been studied recently in some detail on large ribozymes such as group I introns (Bevilacqua *et al.*, 1992; Banerjee *et al.*, 1993; Strobel and Cech, 1994; Zarrinkar and Williamson, 1994, 1996; Downs and Cech, 1996; Emerick *et al.*, 1996; Narlikar and Herschlag, 1996; Cate *et al.*, 1997; Pan *et al.*,

1997; Sclavi *et al.*, 1997, 1998) and RNase P RNA (Zarrinkar *et al.*, 1996; Pan and Sosnick, 1997). Since formation of a distinct tertiary structure is critical for obtaining catalytic activity, folding is at the heart of understanding structure–function relationships in ribozymes. Generally, there is evidence that large RNA molecules fold by a hierarchical pathway consisting of the following sequential steps: (i) fast (within 100 μs) formation of secondary structure domains with metal ions bound in specific sites; (ii) folding (within 10 ms) of tertiary structure scaffolds involving essential metal ions as core for more complex interactions; (iii) interchange (within 1 s) of secondary structure elements as necessary to acquire the native structure; and (iv) metal-ion assisted formation (within 10–1000 s) of tertiary contacts between subdomains to assume the final structure. Sub-populations of the RNA may or may not follow parallel alternative folding pathways.

The results presented in this paper support the idea that folding of small RNA molecules such as the hairpin ribozyme follows a similar pathway, although with fewer kinetic intermediates than the large ribozymes. Folding of the secondary structure in the two independently folding domains is rapid and precedes formation of the closed complex. A flexible region between the two domains acts as a hinge to enable a sharp bend for domain interactions to occur. This global structure is superficially similar to the P4-P6 domain of the *Tetrahymena* group I intron (Cate *et al.*, 1996). Further similarities between the two systems are suggested by recent studies on the dynamics of the P4-P6 domain, involving reversible docking of subdomains separated by a flexible hinge between separately folding subdomains of the molecule, with the inactive conformer consisting of a species in an extended form with coaxial stacking interactions (Szewczak and Cech, 1997). It is noteworthy that tertiary contacts between subdomains of the *Tetrahymena* intron appear to be formed more rapidly (by nearly two orders of magnitude) than those in the hairpin ribozyme (Sclavi *et al.*, 1997, 1998), suggesting that the larger number of contacts between subdomains in P4-P6 might mediate faster docking. In fact, the rate of interchange between hairpin ribozyme conformers is similar to that oberved between populations of alternative stacking conformers in DNA four-way junctions (Miick *et al.*, 1997; Grainger, 1998), providing further support for a model in which the interdomain interactions are specific and functionally important, but weak.

## Materials and methods

### *Synthesis and purification of oligonucleotides*

RNA oligonucleotides were synthesized, and if necessary 3′ phosphorylated, by standard methods using solid-phase phosphoramidite chemistry from Glen Research implemented on an Applied Biosystems 392 DNA/RNA synthesizer. For 3′-end labeling with fluorescein as donor fluorophore for energy transfer, fluorescein CPG column supports were used (1 μmol; Glen Research). For 5′-end labeling with hexachlorofluorescein as the acceptor fluorophore, the commercially available phosphoramidite was used (Glen Research). Deprotection of RNA oligonucleotides was accomplished by the methods of Sproat *et al.* (1995) or Wincott *et al.* (1995), utilizing either methanolic ammonia or a 3:1 mixture of concentrated aqueous ammonia and ethanol to remove the exocyclic amine protection groups and triethylamine trihydrofluoride to remove the 2′-OH silyl protection groups. Fully deprotected, full-length RNA (with or without fluorophores) was isolated by denaturing 20% polyacrylamide gel electrophoresis and subsequent $C_8$-reversed phase HPLC with a gradient of acetonitrile in 0.1 M triethyl ammonium acetate, where fluorophore-coupled RNA was considerably retarded relative to unlabeled RNA. To obtain accurate concentrations for the fluorescein-labeled RNA, the additional absorbance of the fluorophores at 260 nm was taken into account with $A_{260}/A_{492} = 0.3$ for fluorescein and $A_{260}/A_{535} = 0.3$ for hexachlorofluorescein (Bjornson *et al.*, 1994). Non-cleavable substrate analogs were obtained by introducing either a dA or a 2′OMeA modification at the cleavage site (position –1).

### *Steady-state fluorescence kinetic assays*

Steady-state fluorescence spectra and intensities were recorded on an Aminco–Bowman Series 2 (AB2) spectrophotofluorometer from SLM (Rochester, New York) in a cuvette with 3 mm excitation and emission path lengths (150 μl total volume). The water to set up all buffer solutions was degassed and argon-saturated to minimize photobleaching of the fluorophores over extended excitation times. In addition, all buffers {except those containing $[Co(NH_3)_6]^{3+}$} were supplemented with 25 mM DTT as radical quencher and singlet oxygen scavenger (Song *et al.*, 1996). Sample absorbencies were <0.01 at the excitation wavelength, so that inner-filter effects of the solution did not play a significant role. Fluorescein was excited at 485 nm, and fluorescence emission for the kinetic FRET assay was monitored both at 515 and 560 nm by shifting the emission monochromator back and forth. Excitation and emission slits were set to 4 and 8 nm, respectively. Photobleaching of the fluorophores could be neglected. All buffer substances were of ACS reagent quality. Metal salts typically contained chloride as anionic component. Sample temperature was regulated by a VWR 1160A circulating water bath, taking the temperature difference between bath and cuvette content into account.

Ribozyme at a concentration of 20 nM was reconstituted by addition of 200 nM unlabeled 3′ half (3′Rz) to 20 nM of the double-labeled 5′ half (5′Rz) and heating to 70°C for 2 min, followed by cooling to room temperature for 5 min. This procedure ensured that all the fluorophore-labeled strands were incorporated into ribozyme. Since both fluorophores are contained in the same RNA strand, they are always present in a 1:1 ratio. Unless otherwise stated, substrate was added at 200 nM to ensure fast binding by the 5′ half of the ribozyme. Both substrate and ribozyme were separately preincubated in the same reaction buffer at the reaction temperature for 15 min, and hairpin-ribozyme–substrate complex was formed by manually mixing 145 μl ribozyme with 5 μl substrate stock solution in the fluorometer cuvette. Tertiary structure formation was subsequently monitored as fluorescence changes of the two fluorophores over time.

Fluorescence emission values (typically 1 datum $s^{-1}$) for both donor (at 515 nm; $F_{515}$) and acceptor fluorophore (at 560 nm; $F_{560}$) were recorded using the AB2 software package, and a ratio $Q = F_{560}/F_{515}$ reflecting the relative FRET efficiency was calculated simultaneously. To analyze the data, $Q$ was normalized with its value $Q_0$ immediately after formation of the ribozyme–substrate complex [i.e. $(Q–Q_0)/Q_0$ was calculated]. The resulting growth curves generally could be fitted to the single-exponential function $y = y_0 + A(1–e^{-t/\tau})$ to yield the observed docking rate constant $k_{dock,obs} = 1/\tau$ and $A$ as the observed docking amplitude $A_{dock,obs}$. The only exception was docking in the presence of substrate mutant $S(U_{+2}G, dA_{-1})$, where the double-exponential equation $y = y_0 + A_1(1–e^{-t/\tau 1}) + A_2(1–e^{-t/\tau 2})$ had to be used to accurately fit the data, yielding two docking rate constants and amplitudes. Exponential decay curves were fitted to the equation $y = y_0 + A(e^{-(t-t0)/\tau})$, yielding rate constant $k = 1/\tau$ and amplitude $A$.

The dependence of rate constants and amplitudes on the $Mg^{2+}$ concentration were fitted to the cooperative binding equation:

$$f = f_{max} \frac{[Mg^{2+}]^n}{[Mg^{2+}]^n + (K_D^{Mg})^n} \quad (3)$$

to yield an apparent dissociation constant $K_D^{Mg}$ for $Mg^{2+}$ and a cooperativity coefficient $n$. All fits were calculated with Microcal™ Origin™ 4.1 software employing Marquardt–Levenberg non-linear least-squares regression.

### *Fluorescence anisotropy measurements*

Depolarization of fluorescence is dominantly caused by rotational diffusion of the fluorophore and therefore reflects its mobility. Basically, the higher the fluorophore mobility, the more depolarized its emission will be (Lakowicz, 1983). To analyze anisotropies of solutions as a measure for fluorescence polarization, the internal film polarizers of the AB2 spectrophotofluorometer were utilized, and fluorescence intensities

were measured with excitation and emission polarizers subsequently in all four possible combinations of vertical (v, 0°) or horizontal (h, 90°) alignment, $I_{vv}$, $I_{vh}$, $I_{hv}$ and $I_{hh}$. Anisotropy, *A*, then could be calculated as described (Lakowicz, 1983) from

$$A = \frac{I_{vv} - g \cdot I_{vh}}{I_{vv} + 2g \cdot I_{vh}} \quad (4)$$

where $g = I_{hv}/I_{hh}$.

### *Radioactive cleavage and ligation reactions*

5′-$^{32}$P-labeled substrate was prepared by phosphorylation with T4 polynucleotide kinase and [$\gamma^{32}$P]ATP. Radiolabeled substrate and a double-stranded version of the hairpin ribozyme as in Figure 1A, but without fluorophores and including an additional guanosine at the 5′-end, were separately preincubated in reaction buffer (50 mM Tris–HCl, pH 7.5, and varying concentrations of $MgCl_2$) at 25°C for 15 min. To initiate cleavage, a trace (≤1 nM) amount of 5′-$^{32}$P-labeled substrate was added to 100 nM ribozyme. Using up to 1 μM ribozyme gave essentially the same results, indicating that single-turnover or pre-steady-state conditions, with substrate binding significantly faster than cleavage, were maintained. The 5′-cleavage product was separated from uncleaved substrate by denaturing 20% polyacrylamide gel electrophoresis, quantitated and normalized to the sum of the substrate and product bands using a Bio-Rad Molecular Imager System GS-525. The time trace of product formation was fitted to the double-exponential equation $y = y_0 + A_1(1–e^{-t/\tau 1}) + A_2(1–e^{-t/\tau 2})$ as described above. The fast-phase rate constants were plotted over the $Mg^{2+}$ concentration to analyze the data using cooperativity equation 3, as described above. The slow-phase rate constants were discarded as they reflect dissociation of substrate from an inactive ribozyme–substrate conformer (Esteban *et al.*, 1997, 1998). Using the more precious fluorophore-labeled ribozyme gave rate constants that were ~35% lower than those for the unlabeled catalyst.

Simulation of cleavage time traces for different alternative reaction mechanisms was performed using the program HopKINSIM 1.7.2 by Wachsstock and Pollard. Ligation rate constants were determined as described previously (Esteban *et al.*, 1997).

## Acknowledgements

We are grateful to Erika Albinson for excellent technical assistance, David Pecchia for RNA synthesis, Dr A.Raj Banerjee for sharing data on ligation-rate dependence on magnesium concentration prior to publication, Drs Daniel H.Wachsstock, Thomas D.Pollard and Carol A.Fierke for making the kinetic simulation program HopKINSIM 1.7.2 available to us and to Drs José A.Esteban and Joyce E.Heckman for fruitful discussions. This work was supported by grants from the US National Institutes of Health, a Feodor Lynen fellowship from the Alexander von Humboldt foundation to N.G.W., and a postdoctoral fellowship from the Medical Research Council of Canada to K.J.H.

## References

Anderson,P., Monforte,J., Tritz,R., Nesbitt,S., Hearst,J. and Hampel,A. (1994) Mutagenesis of the hairpin ribozyme. *Nucleic Acids Res.*, **22**, 1096–1100.

Banerjee,A.R., Jaeger,J.A. and Turner,D.H. (1993) Thermal unfolding of a group I ribozyme: the low-temperature transition is primarily disruption of tertiary structure. *Biochemistry*, **32**, 153–163.

Bassi,G.S., Murchie,A.I.H., Walter,F., Clegg,R.M. and Lilley,D.M.J. (1997) Ion-induced folding of the hammerhead ribozyme: a fluorescence resonance energy transfer study. *EMBO J.*, **16**, 7481–7489.

Berzal-Herranz,A., Joseph,S., Chowrira,B.M., Butcher,S.E. and Burke,J.M. (1993) Essential nucleotide sequences and secondary structure elements of the hairpin ribozyme. *EMBO J.*, **12**, 2567–2574.

Bevilacqua,P.C., Kierzek,R., Johnson,K.A. and Turner,D.H. (1992) Dynamics of ribozyme binding of substrate revealed by fluorescence-detected stopped-flow methods. *Science*, **258**, 1355–1358.

Bjornson,K.P., Amaratunga,M., Moore,K.J.H. and Lohmann,T.M. (1994) Single-turnover kinetics of helicase-catalyzed DNA unwinding monitored continuously by fluorescence energy transfer. *Biochemistry*, **33**, 14306–14316.

Burke,J.M., Butcher,S.E. and Sargueil,B. (1996) Structural analysis and modifications of the hairpin ribozyme. *Nucleic Acids Mol. Biol.*, **10**, 129–143.

Butcher,S.E. and Burke,J.M. (1994) A photo-cross-linkable tertiary structure motif found in functionally distinct RNA molecules is essential for catalytic function of the hairpin ribozyme. *Biochemistry*, **33**, 992–999.

Butcher,S.E., Heckman,J.E. and Burke,J.M. (1995) Reconstitution of hairpin ribozyme activity following separation of functional domains. *J. Biol. Chem.*, **270**, 29648–29651.

Buzayan,J.M., Gerlach,W.L. and Bruening,G. (1986) Non-enzymatic cleavage and ligation of RNAs complementary to a plant virus satellite RNA. *Nature*, **323**, 349–353.

Cate,J.H., Gooding,A.R., Podell,E., Zhou,K., Golden,B.L., Kundrot,C.E., Cech,T.R. and Doudna,J.A. (1996) Crystal structure of a group I ribozyme domain: principles of RNA packing. *Science*, **273**, 1678–1685.

Cate,J.H., Hanna,R.L. and Doudna,J.A. (1997) A magnesium ion core at the heart of a ribozyme domain. *Nature Struct. Biol.*, **4**, 553–558.

Chowrira,B.M. and Burke,J.M. (1992) Extensive phosphorothioate substitution yields highly active and nuclease-resistant hairpin ribozymes. *Nucleic Acids Res.*, **20**, 2835–2840.

Chowrira,B.M., Berzal-Herranz,A. and Burke,J.M. (1991) Novel guanosine requirement for catalysis by the hairpin ribozyme. *Nature*, **354**, 320–322.

Chowrira,B.M., Berzal-Herranz,A. and Burke,J.M. (1993a) Ionic requirements for RNA binding, cleavage, and ligation by the hairpin ribozyme. *Biochemistry*, **32**, 1088–1095.

Chowrira,B.M., Berzal-Herranz,A., Keller,C.F. and Burke,J.M. (1993b) Four ribose 2′-hydroxyl groups essential for catalytic function of the hairpin ribozyme. *J. Biol. Chem.*, **268**, 19458–19462.

DeYoung,M.B., Siwkowski,A.M., Lian,Y. and Hampel,A. (1995) Catalytic properties of hairpin ribozymes derived from chicory yellow mottle virus and arabis mosaic virus satellite RNAs. *Biochemistry*, **34**, 15785–15791.

Downs,W.D. and Cech,T.R. (1996) Kinetic pathway for folding of the *Tetrahymena* ribozyme revealed by three UV-inducible crosslinks. *RNA*, **2**, 718–732.

Draper,D.E. (1996) Parallel worlds. *Nature Struct. Biol.*, **3**, 397–400.

Earnshaw,D.J. and Gait,M.J. (1997) Progress toward the structure and therapeutic use of the hairpin ribozyme. *Antisense Nucleic Acid Drug Dev.*, **7**, 403–411.

Earnshaw,D.J., Masquida,B., Müller,S., Sigurdsson,S.T., Eckstein,F., Westhof,E. and Gait,M.J. (1997) Inter-domain cross-linking and molecular modelling of the hairpin ribozyme. *J. Mol. Biol.*, **247**, 1–16.

Emerick,V.L., Pan,J. and Woodson,S.A. (1996) Analysis of rate-determining conformational changes during self-splicing of the *Tetrahymena* intron. *Biochemistry*, **35**, 13469–13477.

Esteban,J.A., Banerjee,A.R. and Burke,J.M. (1997) Kinetic mechanism of the hairpin ribozyme. Identification and characterization of two nonexchangeable conformations. *J. Biol. Chem.*, **272**, 13629–13639.

Esteban,J.A., Walter,N.G., Kotzorek,G., Heckman,J.E. and Burke,J.M. (1998) Structural basis for heterogeneous kinetics: Re-engineering the hairpin ribozyme. *Proc. Natl Acad. Sci. USA*, in press.

Feldstein,P.A. and Bruening,G. (1993) Catalytically active geometry in the reversible circularization of mini-monomer RNAs derived from the complementary strand of tobacco ringspot virus satellite RNA. *Nucleic Acids Res.*, **21**, 1991–1998.

Feldstein,P.A., Buzayan,J.M. and Bruening,G. (1989) Two sequences participating in the autocatalytic processing of satellite tobacco ringspot virus complementary RNA. *Gene*, **82**, 53–61.

Grainger,R.J., Murchie,A.I.H. and Lilley,D.M.J. (1998) Exchange between stacking conformers in a four-way DNA junction. *Biochemistry*, **37**, 23–32.

Hampel,A. and Cowan,J.A. (1997) A unique mechanism for RNA catalysis: the role of metal cofactors in hairpin ribozyme cleavage. *Chem. Biol.*, **4**, 513–517.

Hampel,A. and Tritz,R. (1989) RNA catalytic properties of the minimum (–)sTRSV sequence. *Biochemistry*, **28**, 4929–4933.

Hegg,L.A. and Fedor,M.J. (1995) Kinetics and thermodynamics of intermolecular catalysis by hairpin ribozymes. *Biochemistry*, **34**, 15813–15828.

Johnson,K.A. (1992) Transient-state kinetic analysis of enzyme reaction pathways. In Sigman,D. (ed.), *The Enzymes*. Vol. 20. Academic Press, New York, NY, pp. 1–61.

Komatsu,Y., Koizumi,M., Nakamura,H. and Ohtsuka,E. (1994) Loop-size variation to probe a bent structure of a hairpin ribozyme. *J. Am. Chem. Soc.*, **116**, 3692–3696.

Lakowicz,J.R. (1983) *Principles of Fluorescence Spectroscopy.* Plenum Press, New York, NY.
Long,D.M. and Uhlenbeck,O.C. (1993) Self-cleaving catalytic RNA. *FASEB J.*, **7**, 25–30.
Miick,S.M., Fee,R.S., Millar,D.P. and Chazin,W.J. (1997) Crossover isomer bias is the primary sequence-dependent property of immobilized Holliday junctions. *Proc. Natl Acad. Sci. USA*, **94**, 9080–9084.
Morrison,L.E. and Stols,L.M. (1993) Sensitive fluorescence-based thermodynamic and kinetic measurements of DNA hybridization in solution. *Biochemistry*, **32**, 3095–3104.
Narlikar,G.J. and Herschlag,D. (1996) Isolation of a local tertiary folding transition in the context of a globally folded RNA. *Nature Struct. Biol.*, **3**, 701–710.
Nesbitt,S., Hegg,L.A. and Fedor,M.J. (1997) An unusual mechanism for hairpin ribozyme catalysis: pH and metal ion independence. *Chem. Biol.*, **4**, 619–630.
Pan,J., Thirumalai,D. and Woodson,S.A. (1997) Folding of RNA involves parallel pathways. *J. Mol. Biol.*, **273**, 7–13.
Pan,T. and Sosnick,T.R. (1997) Intermediates and kinetic traps in the folding of a large ribozyme revealed by circular dichroism and UV absorbance spectroscopies and catalytic activity. *Nature Struct. Biol.*, **4**, 931–938.
Parkhurst,K.M and Parkhurst,L.J. (1995) Kinetic studies by fluorescence resonance energy transfer employing a double-labeled oligonucleotide: hybridization to the oligonucleotide complement and a single-stranded DNA. *Biochemistry*, **34**, 285–292.
Perkins,T.A., Wolf,D.E. and Goodchild,J. (1996) Fluorescence resonance energy transfer analysis of ribozyme kinetics reveals the mode of action of a facilitator oligonucleotide. *Biochemistry*, **35**, 16370–16377.
Sclavi,B., Woodson,S., Sullivan,M., Chance,M.R. and Brenowitz,M. (1997) Time-resolved synchrotron X-ray 'footprinting', a new approach to the study of nucleic acid structure and function: application to protein–DNA interactions and RNA folding. *J. Mol. Biol.*, **266**, 144–159.
Sclavi,B., Woodson,S., Sullivan,M., Chance,M.R. and Brenowitz,M. (1998) Visualizing RNA folding at millisecond intervals by X-ray footprinting. *Science*, in press.
Sigurdsson,S.T., Thomson,J.B. and Eckstein,F. (1998) Small ribozymes. In Simons,R.W. (ed.), *RNA Structure and Function*. Cold Spring Harbor Laboratory Press, Cold Spring Harbor, NY, pp. 339–376.
Song,L., Varma,C.A.G.O., Verhoeven,J.W. and Tanke,H.J. (1996) Influence of the triplet excited state on the photobleaching kinetics of fluorescein in microscopy. *Biophys. J.*, **70**, 2959–2968.
Sproat,B., Colonna,F., Mullah,B., Tsou,D., Andrus,A., Hample,A. and Vinayak,R. (1995) An efficient method for isolation and purification of oligoribonucleotides. *Nucl. Nucl.*, **14**, 255–273.
Strobel,S.A. and Cech,T.R. (1994) Translocation of an RNA duplex on a ribozyme. *Nature Struct. Biol.*, **1**, 13–17.
Szewczak,A.A. and Cech,T.R. (1997) An RNA internal loop acts as a hinge to facilitate ribozyme folding and catalysis. *RNA*, **3**, 838–849.
Turner,D.H., Li,Y., Fountain,M., Profenno,L. and Bevilacqua,P.C. (1996) Dynamics of a group I ribozyme detected by spectroscopic methods. *Nucleic Acids Mol. Biol.*, **10**, 19–32.
Tuschl,T., Gohlke,C., Jovin,T.M., Westhof,E. and Eckstein,F. (1994) A three-dimensional model for the hammerhead ribozyme based on fluorescence measurements. *Science*, **266**, 785–789.
Walter,N.G. and Burke,J.M. (1997) Real-time monitoring of hairpin ribozyme kinetics through base-specific quenching of fluorescein-labeled substrates. *RNA*, **3**, 392–404.
Walter,N.G. and Burke,J.M. (1998) The hairpin ribozyme: structure, assembly and catalysis. *Curr. Opin. Chem. Biol.*, **2**, 24–30.
Walter,N.G., Albinson,E. and Burke,J.M. (1997) Probing structure formation in the hairpin ribozyme using fluorescent substrate analogs. *Nucleic Acids Symp. Ser.*, **36**, 175–177.
Welch,P.J., Hampel,A., Barber,J., Wong-Staal,F. and Yu,M. (1996) Inhibition of HIV replication by the hairpin ribozyme. *Nucleic Acids Mol. Biol.*, **10**, 315–327.
Wincott,F. *et al.* (1995) Synthesis, deprotection, analysis and purification of RNA and ribozymes. *Nucleic Acids Res.*, **23**, 2677–2684.
Wu,P. and Brand,L. (1994) Resonance energy transfer: methods and applications. *Anal. Biochem.*, **218**, 1–13.
Yang,M., Ghosh,S.S. and Millar,D.P. (1994) Direct measurement of thermodynamic and kinetic parameters of DNA triple helix formation by fluorescence spectroscopy. *Biochemistry*, **33**, 15329–15337.
Young,K.J., Gill,F. and Grasby,J.A. (1997) Metal ions play a passive role in the hairpin ribozyme catalysed reaction. *Nucleic Acids Res.*, **25**, 3760–3766.
Zarrinkar,P.P. and Williamson,J.R. (1994) Kinetic intermediates in RNA folding. *Science*, **265**, 918–924.
Zarrinkar,P.P. and Williamson,J.R. (1996) The kinetic folding pathway of the *Tetrahymena* ribozyme reveals possible similarities between RNA and protein folding. *Nature Struct. Biol.*, **3**, 432–438.
Zarrinkar,P.P., Wang,J. and Williamson,J.R. (1996) Slow folding kinetics of RNase P RNA. *RNA*, **2**, 564–573.

*Received January 26, 1998; revised February 17, 1998; accepted February 24, 1998*